



Cite this: *Phys. Chem. Chem. Phys.*,  
2016, **18**, 24285

# Performance enhancement of organic photovoltaic devices enabled by Au nanoarrows inducing surface plasmonic resonance effect

Shujun Li,<sup>ab</sup> Zhiqi Li,<sup>a</sup> Xinyuan Zhang,<sup>a</sup> Zhihui Zhang,<sup>a</sup> Chunyu Liu,<sup>a</sup> Liang Shen,<sup>a</sup> Wenbin Guo<sup>\*a</sup> and Shengping Ruan<sup>a</sup>

The surface plasmon resonance (SPR) effect of metal nanoparticles is widely employed in organic solar cells to enhance device performance. However, the light-harvesting improvement is highly dependent on the shape of the metal nanoparticles. In this study, the significantly enhanced performance upon incorporation of Au nanoarrows in solution-processed organic photovoltaic devices is demonstrated. Incorporating Au nanoarrows into the ZnO cathode buffer layer results in superior broadband optical absorption improvement and a power conversion efficiency of 7.82% is realized with a 27.3% enhancement compared with the control device. The experimental and theoretical results indicate that the introduction of Au nanoarrows not only increases optical trapping by the SPR effect but also facilitates exciton generation, dissociation, and charge transport inside the thin film device.

Received 20th June 2016,  
Accepted 3rd August 2016

DOI: 10.1039/c6cp04302j

www.rsc.org/pccp

## 1. Introduction

Predictions of limited fossil fuels and environmental issues caused by them have motivated a rapid growth in research on new energy development, and clean and exhaustless solar energy may be the most ideal alternative to fossil fuels. In the last decade, organic photovoltaic devices (OPVs) have attracted great attention due to their unique properties, such as low-fabrication-cost, solution processability, flexibility, lightweight, and potential for large-scale manufacture.<sup>1–4</sup> Recently, studies on OPVs have covered almost all aspects, including materials synthesis and design, interfacial engineering, nanoparticles doping, light harvesting methods, tandem structures, and so on, which have resulted in a great power conversion efficiency (PCE) increase of more than 10%. However, the relatively lower PCE is a bottleneck that causes OPVs to be far away from commercial application compared to inorganic solar cells.

Generally, the low PCE of OPVs is mainly attributed to two factors. On the one hand, it is really a great waste to utilize only a limited range of the solar spectrum, due to the narrow absorption spectra of polymer semiconductors. On the other hand, the poor efficiency of excitation separation and charge transfer in an organic active layer leads to a relatively lower

photocurrent. Usually, the optimum thickness of the active layer for an OPV device is about 100–200 nm, or even less, leading to low optical absorption. Hence, it is a key point to develop novel approaches to enhance light trapping without increasing the film thickness, so as to avoid the increase of the charge recombination.<sup>5–7</sup>

It has been proved that the introduction of an optical spacer that spatially redistributes the light intensity in the OPVs can realize enhanced light absorption.<sup>8–11</sup> Also, the introduction of periodic nanostructures and relative changes in the device symmetry can increase the optical path length in the active layer.<sup>12–16</sup> Moreover, microcavity and photonic crystal effects have been proposed to effectively trap light in OPVs.<sup>17–22</sup> Lately, metallic nanoparticles (NPs) such as Cu, Ag, Pt, and Au have been introduced into OPVs, and notably improved the photocurrent by utilizing both the surface plasmon resonance (SPR) effects<sup>23–29</sup> and scattering effects.<sup>30–34</sup> SPR is referred to as the coherent, collective oscillation of conduction electrons surrounding the metallic surface, which can also enhance the degree of exciton dissociation.<sup>35</sup> Incorporation of noble metallic NPs in OPVs can facilitate light trapping enhancement without increasing the thickness of the active layers or buffer layers. Recently, zinc oxide (ZnO), having the great advantage of the excellent ability to form numerous morphologies, in addition to excellent electron affinity, solution processability, and good transparency, has been widely used as a cathode buffer layer. In this study, Au nanoarrows (NAs) were added into the ZnO buffer layer of OPVs based on poly[*N*-900-hepta-decanyl-2,7-carbazole-*alt*-5,5-(40,70-di-2-thienyl-20,10,30-benzothiadiazole)] (PCDTBT) and [6,6]-phenyl C<sub>71</sub>-butyric

<sup>a</sup> State Key Laboratory on Integrated Optoelectronics, Jilin University, College of Electronic Science and Engineering, 2699 Qianjin Street, Changchun 130012, People's Republic of China. E-mail: guowb@jlu.edu.cn

<sup>b</sup> Changchun Institute of Optics, Fine Mechanics and Physics, Chinese Academy of Sciences, 3888 Eastern South Lake Road, Changchun, 130033, China

acid methyl ester (PC<sub>71</sub>BM), and the cooperative PCE was increased from 6.14% to 7.82%, accounting for a 27.4% enhancement. Detailed research attests that the excitation of SPR triggered by Au NAs significantly enhanced the degree of light absorption, as well as the degree of exciton dissociation.

## 2. Experimental section

### 2.1 Preparation of the ZnO cathode buffer layer

ZnO nanoparticles (NPs) were prepared according to previous reports.<sup>36,37</sup> The ZnO NPs were then dissolved in chloroform to obtain a solution with a concentration of 80 mg mL<sup>-1</sup>, on average. After that, a mixture of chloroform with a small amount methanol (10% vol) was added to the original solution and the concentration of 15 mg mL<sup>-1</sup> ZnO was subsequently obtained. The Au NAs were synthesized as described in our previous paper.<sup>38</sup> Fig. 1(a) gives the transmission electron microscope (TEM) images of Au NAs, and the diameter and length of Au NAs are about 15 and 60 nm, respectively. Finally, the two solutions were mixed and stirred for 24 hours, and the ZnO cathode buffer layer solutions containing different concentrations of Au NAs were obtained, and the corresponding weight ratios of Au NAs and ZnO were 0, 0.5, 1.0, 1.5, and 2.0 wt%, respectively.

### 2.2 Device fabrication and characterization

The OPVs containing a ZnO cathode buffer layer with different ratios of Au NAs were fabricated with the structure of indium tin oxide (ITO)/zinc oxide (ZnO)/PCDTBT:PC<sub>71</sub>BM/molybdenum oxide (MoO<sub>3</sub>)/silver (Ag) on clean ITO/glass substrates, schematically shown in Fig. 1(b). The patterned ITO/glass substrates were cleaned with acetone, alcohol and deionized water under ultrasonic processing for 20 minutes, respectively. The ZnO:NA solutions were then spin-cast at 2000 revolutions per minute (rpm) onto the substrates. The PCDTBT:PC<sub>71</sub>BM blend solution was subsequently spin-cast on the top of the ZnO layer at 1000 rpm and annealed at 70 °C for 10 minutes in an atmosphere of argon. Next, MoO<sub>3</sub> acting as the hole transport layer was deposited onto the active layer film through thermal evaporation with a thickness of 4 nm. Finally, the device was finished with 110 nm Ag deposited as the anode. Moreover, single-electron devices with the structure of ITO/ZnO/PCDTBT:PC<sub>71</sub>BM/BCP/Ag were also fabricated using the same method, to investigate the effect of Au NAs on the device conductivity. The photovoltaic characteristics were determined using a computer-programmed Keithley 2401 source meter with an intensity of 100 mW cm<sup>-2</sup> and an Oriel

300 W solar simulator. The external quantum efficiency (EQE) spectra of the devices were tested with a Crowntech Qtest Station 1000AD. Atomic force microscope (AFM) images were obtained using a Solver Scanning Probe microscope in tapping mode. Impedance spectroscopy was measured with an impedance analyzer (Wayne Kerr Electronics 6520B).<sup>39,40</sup>

## 3. Results and discussion

To investigate the effect of Au NAs on the morphology of ZnO film, the AFM images with the structure of silicon substrate/ZnO:NA were measured. Fig. 2 illustrates AFM images of the ZnO buffer layer without and with 1.5 wt% NAs doping. The root-mean-squared (RMS) roughness of pristine ZnO film (Fig. 2a) was observed to be 1.11 nm, while ZnO film mixed with 1.5 wt% NAs exhibited a higher RMS (Fig. 2b). The enlarged RMS would provide improved interfacial adhesion between the ZnO and active layer, and consequently give rise to facilitated charge transport at the ITO/active layer interface. Improved interfacial coherence and enhanced electrical conductivity of the ZnO reduced the energy barrier at the ZnO/active layer interface. In addition, the ZnO film with 1.5 wt% Au NAs presents an obvious and homogeneous interfacial phase (Fig. 2b), which cannot be observed from the buffer layer without Au NAs (Fig. 2a). The doped films show uniformly percolated structures, which are beneficial to the contact with active layer.<sup>41</sup> It is well recognized that the continuous interpenetrating interlayer with proper domain size plays an important role in exciton separation and charge transport.<sup>42,43</sup>

To explore the role of Au NAs, ZnO buffer layers with different concentrations of Au NAs (0, 0.5, 1.0, 1.5, 2.0 wt%) were employed in OPVs, and the corresponding *J-V* characteristics are displayed in Fig. 3a. The detailed performance parameters including short-circuit current density (*J*<sub>sc</sub>), open-circuit voltage (*V*<sub>oc</sub>), fill factor (FF), and PCE are listed in Table 1, which are typical average values for 32 devices. It can be seen that the control device without NAs has a relatively lower efficiency, including a *V*<sub>oc</sub> of 0.85 V, a *J*<sub>sc</sub> of 14.70 mA cm<sup>-2</sup>, a FF of 49.1%, and a calculated PCE of 6.14%. As expected, after introducing Au NAs into the ZnO electron transport layer, the device efficiency was greatly improved. In particular, the OPV device with 1.5 wt% Au NAs showed the best PCE of 7.82% with a *V*<sub>oc</sub> of 0.85 V, a *J*<sub>sc</sub> of 17.40 mA cm<sup>-2</sup>, and a FF of 52.9%. The dramatically increased *J*<sub>sc</sub> and PCE can be ascribed to

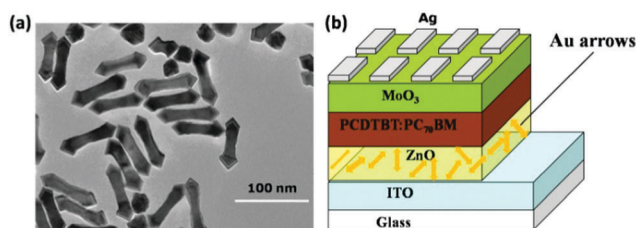


Fig. 1 (a) TEM image of Au nanoarrows, (b) schematic device structure of inverted polymer solar cells embedded by Au NAs.

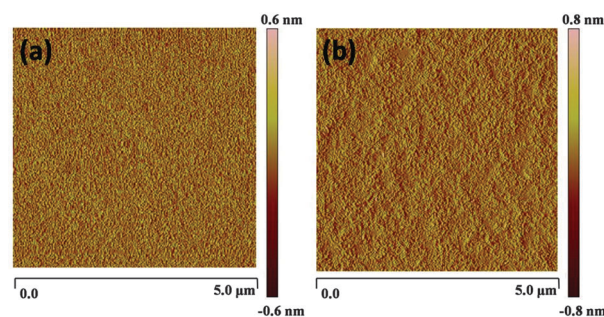


Fig. 2 AFM morphology images of ZnO films (a) without and (b) with 1.5 wt% Au NAs incorporation.

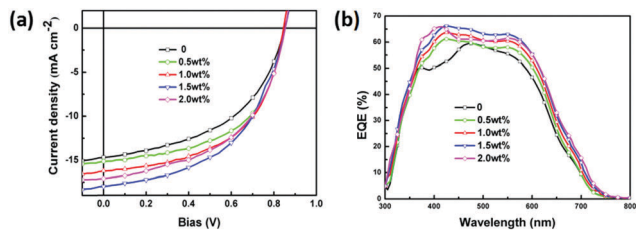


Fig. 3 (a)  $J$ - $V$  characteristics and (b) EQE spectra of inverted polymer photovoltaic devices with various concentrations of Au NAs doped in ZnO buffer layers.

**Table 1** The detailed performance parameters of devices without or with different ratios of Au nanoarrows doping, under  $100 \text{ mW cm}^{-2}$  simulated AM1.5G in ambient air

Au (wt%)	$V_{oc}$ (V)	$J_{sc}$ ( $\text{mA cm}^{-2}$ )	FF (%)	PCE (%)
0	$0.85 \pm 0.01$	$14.70 \pm 0.01$	49.1	$6.14 \pm 0.11$
0.5	$0.85 \pm 0.01$	$15.10 \pm 0.01$	54.8	$7.08 \pm 0.08$
1.0	$0.85 \pm 0.01$	$16.20 \pm 0.04$	54.6	$7.48 \pm 0.13$
1.5	$0.85 \pm 0.01$	$17.40 \pm 0.03$	52.9	$7.82 \pm 0.05$
2.0	$0.85 \pm 0.01$	$17.10 \pm 0.02$	51.1	$6.71 \pm 0.12$

the light absorption enhancement and charge transport improvement induced by Au NAs. It is worth noting that the  $V_{oc}$  and FF of all devices keep almost no change, regardless of incorporating Au NAs or not, indicating that the inclusion of Au NAs did not change the Fermi level of the ZnO layer and built-in potential of the device.<sup>42–45</sup> To prove that the enhancement of  $J_{sc}$  originated from the increasing light-harvesting, the EQE measurements of all devices with and without Au NAs were performed and shown in Fig. 3b. It can be clearly seen that the EQE of devices with Au NAs exhibits a significant increase in a broader wavelength region of 380–650 nm compared to the control device. Additionally, the peak value of the EQE for the device with 1.5 wt% Au NAs reached 78%, and the value of the control device was 58%, providing direct evidence that NAs induced SPR can enhance  $J_{sc}$ .

In order to unravel the operating mechanism of Au NAs on the optical absorption enhancement, the theoretical analog calculations of electric field profiles in ZnO film doped with Au NAs were carried out by the finite-difference time-domain (FDTD) method. Fig. 4 shows the distribution of field intensity around Au NAs at the wavelength of 500 nm, which corresponds to the peaks of EQE enhancements in Fig. 3b, including the end view (Fig. 4a) and side view (Fig. 4b). The magnitude of the enhanced electric field was shown by the color scale, and the SPR effect of Au NAs in ZnO film was really triggered, which can diffuse into the active layer. This indicates that the resonant near-field enhancement is the primary mechanism contributing to the enhanced absorption, with a small additional contribution from enhanced far-field scattering into the optical modes of the device. It has been announced that Au and Ag nanoparticles can act as effective antennas for the incident light that stores photon energy in a SPR mode.

To confirm the actual function of Au NAs on the light-harvesting improvement of OPVs, UV-vis absorption spectra of the ZnO layer containing different amounts of Au NAs based

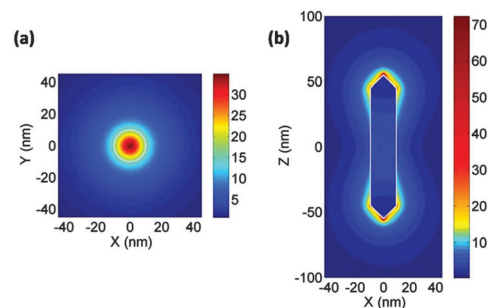


Fig. 4 Electric field enhancement induced by the SPR effect of Au NAs in the ZnO cathode buffer layer, (a) the electric profile in the end view, (b) the electric profile in the side view.

on glass/ITO substrates were tested and shown in Fig. 5a. It can be seen that the light absorption of ZnO films doped with NAs is almost unchanged, except for the doping concentration of 2.0 wt%. In addition, the absorption spectrum of the complete devices containing different amounts of Au NAs was measured (Fig. 5b), and the calculated difference is exhibited in Fig. 5c. As is shown in Fig. 5c, the incorporation of Au NAs in the ZnO layer leads to a great optical absorption for the active layer covering the wavelength range from 400 to 650 nm. Therefore, the light trapping enhancement of the active layer was attributed to the SPR and scattering effect of Au NAs. What is more, Au NAs embedded in the ZnO layer can act as an antenna and scatter light into the active layer, leading to the increase of the optical path within the active layer and the possibility of photon utilization.

To deeply understand the effect of Au NAs on charge transport properties, steady-state photoluminescence spectra of ZnO films with and without Au NAs were also obtained, and the results are shown in Fig. 6a. The PL spectra signals were corrected with the absorption spectra of ZnO at the wavelength of 450 nm. After introducing Au NAs, PL quenching was observed covering the wavelength region of 350–600 nm. As we know, PL occurs accompanied by the depletion of photon-generated charge carriers. Therefore, the PL decrease implies that the photon-generated radiative loss of electrons and holes is reduced, which means that the incorporation of Au NAs in ZnO will benefit the free charge carriers transport and collection. In addition to the significant improvement in  $J_{sc}$ , FF of the doping devices increases moderately, indicating that the charge transport properties of the whole device are also improved. In order to make it clear, electron-only devices with the structure of ITO/ZnO(Au NAs)/PCDTBT:PC<sub>71</sub>BM/BCP/Ag were also fabricated, and  $J$ - $V$  characteristics are shown in Fig. 6b. The OPVs doped with different concentrations of Au NAs indicate larger current density compared to the control device, and the largest current arises at the concentration of 2.0%. To better explain the improved charge transfer properties, the electron mobility was calculated using the space-charge-limited current (SCLC) model, and it increased from  $2.2 \times 10^{-4} \text{ cm}^2 \text{ V}^{-1} \text{ s}^{-1}$  to  $2.4 \times 10^{-3} \text{ cm}^2 \text{ V}^{-1} \text{ s}^{-1}$ , suggesting that the incorporation of Au NAs can greatly improve the electron carrier mobility.

To demonstrate the concentration dependence of device performance on Au NAs, the complex impedance spectra for

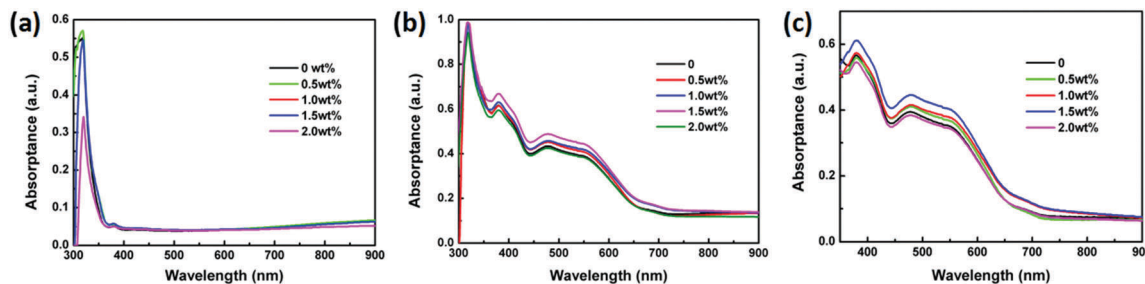


Fig. 5 (a) The absorption spectra of ZnO films doped with various concentrations of Au NAs, (b) the light-harvesting of completed OPVs with different ratios of Au NAs in ZnO layers, (c) the light trapping difference of pure PCDTBT:PC<sub>71</sub>BM on the ZnO films with various amounts of Au NAs.

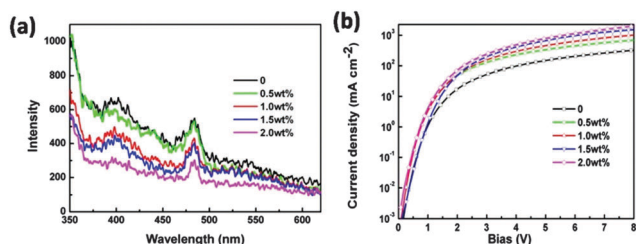


Fig. 6 (a) The PL spectra of ZnO films incorporating various concentrations of Au NAs, (b)  $J$ - $V$  characteristics of single electron devices with various amounts of Au NAs under dark conditions.

devices without and with different concentrations of Au NAs were measured under dark conditions (Fig. 7), which are beneficial for obtaining valuable information on kinetics and energetic processes that govern the device performance.<sup>46</sup> Also, it is an essential tool to observe bulk and electrical properties that cannot be observed in the direct current regime.<sup>47</sup> The measurement was done under an alternating current signal of open circuit voltage in the frequency range from 0.1 Hz to 1 MHz. To better explain the electrical behavior of such a device structure, we propose the equivalent electrical circuit model (Fig. 7a), and the corresponding equation is as follows:

$$Z = R_s + \frac{1}{\frac{1}{R_r} + j\omega C_\mu} \quad (1)$$

where  $C_\mu$  is the chemical capacitance (connected to carrier storage),  $R_r$  is the recombination resistance (derivative of the carrier recombination flux) response,  $R_1$  is the transport-related resistance,  $R_r$  is related to recombination resistance, and  $R_0$  is

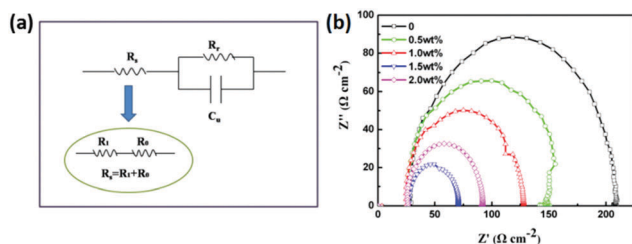


Fig. 7 (a) The equivalent circuit model and (b) Impedance spectra of OPV devices with different concentrations of Au NAs incorporated in ZnO buffer layers.

the anode interface, buffer layer, and wire resistance for OPVs. The series resistance ( $R_s$ ) was introduced as  $R_s = R_1 + R_0$ . Fig. 7b shows the Nyquist curves of the impedance spectra for undoped and doped devices. An apparent change is observed in the doped devices. The real impedance is decreased with increased doping concentrations.  $R_s$  and  $R_r$  significantly trend toward decrease, owing to the incorporation of Au NAs, resulting in an increased FF. The capacitance  $C_\mu$  is attributed to the depletion region chemical capacitance, due to the connection to carrier storage. This capacitance follows the Mott-Schottky expression as follows:

$$C_\mu^{-2} = \frac{2(V_{bi} - V)}{A^2 e \epsilon_0 \epsilon_D N} \quad (2)$$

Charge carrier density can be calculated by the following:

$$N = \frac{1}{e} A d \int_{\text{dark}}^{V_{oc}} C(V) dV \quad (3)$$

where  $e$  is elementary charge,  $A$  is the device area,  $d$  is the thickness of the active layer, and  $C$  is the chemical capacitance. Higher chemical capacitance was obtained after incorporation of Au NAs, resulting in a higher electron concentration. The higher electron mobility and charge carrier concentration in the doped device suggest that more efficient charges were extracted by electrodes.

## 4. Conclusion

In conclusion, the SPR effect induced high performance OPVs have been demonstrated *via* embedding Au NAs into the ZnO interface layer. The results of  $J_{sc}$  and EQE measurements reveal that Au NAs significantly improve light-harvesting in the visible range, yielding a PCE enhancement. Incorporation of the Au NAs improved the charge transport and collection properties, which guarantees the better performance of doping devices. Also, the addition of high-conductivity Au NAs resulted in low series resistance and larger resultant photocurrent. The optimized doping concentration of 1.5 wt% led to a 27.3% increase of PCE, and the highest PCE of 7.82% was achieved. This study offers an effective method to improve the efficiency of OPVs.

## Acknowledgements

The authors are grateful to National Natural Science Foundation of China (61275035, 61370046, 11574110), the Opened Fund of the State Key Laboratory on Integrated Optoelectronics (IOSKL2013KF10) for the support to the work.

## Notes and references

- 1 F. C. Krebs, J. Fyenbo and M. Jørgensen, *J. Mater. Chem.*, 2010, **20**, 8994.
- 2 T. D. Nielsen, C. Cruickshank, S. Foged, J. Thorsen and F. C. Krebs, *Sol. Energy Mater. Sol. Cells*, 2010, **94**, 1553.
- 3 C. Edwards, A. Arbabi, G. Popescu and L. L. Goddard, *Light: Sci. Appl.*, 2012, **1**, e30.
- 4 F. C. Frebs, J. Fyenbo and M. Jørgensen, *J. Mater. Chem.*, 2010, **20**, 8994.
- 5 V. Shrotriya, E. H. E. Wu, G. Li, Y. Yao and Y. Yang, *Appl. Phys. Lett.*, 2006, **88**, 064104.
- 6 K. S. Lee, J. A. Lee, B. A. Mazor and S. R. Forst, *Light: Sci. Appl.*, 2015, **4**, e288.
- 7 A. Yakimov and S. R. Forrest, *Appl. Phys. Lett.*, 2002, **80**, 1667.
- 8 F. C. Chen, J. L. Wu and Y. Hung, *Appl. Phys. Lett.*, 2010, **96**, 193304.
- 9 J. Gilot, I. Barbu, M. M. Wienk and R. A. J. Janssen, *Appl. Phys. Lett.*, 2007, **91**, 113520.
- 10 J. Y. Kim, S. H. Kim, H. H. Lee, K. Lee, W. L. Ma, X. Gong and A. J. Heeger, *Adv. Mater.*, 2006, **18**, 572.
- 11 A. Roy, S. H. Park, S. Cowan, M. H. Tong, S. N. Cho, K. Lee and A. J. Heeger, *Appl. Phys. Lett.*, 2009, **95**, 013302.
- 12 K. Tvingstedt, V. Andersson, F. Zhang and O. Inganäs, *Appl. Phys. Lett.*, 2007, **91**, 123514.
- 13 Y. H. Zhou, F. L. Zhang, K. Tvingstedt, W. J. Tian and O. Inganäs, *Appl. Phys. Lett.*, 2008, **93**, 033302.
- 14 B. C. Park, S. H. Yun, C. Y. Cho, Y. C. Kim, J. C. Shin, H. G. Jeon, Y. H. Huh, I. C. Hwang, K. Y. Baik and Y. I. Lee, *Light: Sci. Appl.*, 2014, **3**, e222.
- 15 C. Cocoyer, L. Rocha, L. Sicot, B. Geffroy, R. de Bettignies, C. Sentein, C. Fiorini-Debuisschert and P. Raimond, *Appl. Phys. Lett.*, 2006, **88**, 133108.
- 16 S. I. Na, S. S. Kim, J. Jo, S. H. Oh, J. Kim and D. Y. Kim, *Adv. Funct. Mater.*, 2008, **18**, 3956.
- 17 D. H. Ko, J. R. Tumbleston, L. Zhang, S. Williams, J. M. DeSimone, R. Lopez and E. T. Samulski, *Nano Lett.*, 2009, **9**, 2742.
- 18 J. R. Tumbleston, D. H. Ko, E. T. Samulski and R. Lopez, *Opt. Express*, 2009, **17**, 7670.
- 19 Y. B. Long, *Appl. Phys. Lett.*, 2009, **95**, 193301.
- 20 X. Chen, B. H. Jia, Y. A. Zhang and M. Gu, *Light: Sci. Appl.*, 2013, **2**, e92.
- 21 Z. C. Holman, S. D. Wolf and C. Ballif, *Light: Sci. Appl.*, 2013, **2**, e106.
- 22 Y. H. Su, Y. F. Ke, S. L. Cai and Q. Y. Yao, *Light: Sci. Appl.*, 2012, **1**, e14.
- 23 Q. Gan, F. J. Bartoli and Z. H. Kafafi, *Adv. Mater.*, 2013, **25**, 2385.
- 24 Y. M. Sung, Y. C. Lai, M. F. Tsai, H. H. Hsieh, M. H. Yang, P. P. Wei, C. Yeh, F. C. Hsu and Y. F. Chen, *J. Mater. Chem. C*, 2016, **4**, 513.
- 25 G. Kakavelakis, I. Vangelidis, A. H. Jungemann, A. G. Kanaras, E. Lidorikis, E. Stratakis and E. Kymakis, *Adv. Energy Mater.*, 2016, **6**, 1501640.
- 26 M. N. Yao, X. Jia, Y. Liu, W. B. Guo, L. Shen and S. P. Ruan, *ACS Appl. Mater. Interfaces*, 2015, **7**, 18866.
- 27 M. Krassas, G. Kakavelakis, M. M. Stylianakis, N. Vaenas, E. Stratakis and E. Kymakis, *RSC Adv.*, 2015, **5**, 71704.
- 28 M. N. Yao, P. Shen, Y. Liu, B. Y. Chen, W. B. Guo, S. P. Ruan and L. Shen, *ACS Appl. Mater. Interfaces*, 2016, **8**, 6183.
- 29 L. Y. Lu, Z. Q. Luo, T. Xu and L. P. Yu, *Nano Lett.*, 2013, **13**, 59.
- 30 L. Z. Chen, W. C. H. Choy, E. I. Wei and W. E. I. Sha, *Appl. Phys. Lett.*, 2013, **102**, 251112.
- 31 S. W. Baek, J. Noh, C. H. Lee, B. S. Kim, M. K. Seo and J. Y. Lee, *Sci. Rep.*, 2013, **3**, 1726.
- 32 O. Blum and N. T. Shaked, *Light: Sci. Appl.*, 2015, **4**, e322.
- 33 D. Lepage, A. Jimenez, J. Beauvais and J. J. Dubowski, *Light: Sci. Appl.*, 2012, **1**, e28.
- 34 W. E. I. Sha, W. C. H. Choy, Y. G. Liu and C. C. Weng, *Appl. Phys. Lett.*, 2011, **99**, 113304.
- 35 J. L. Wu, F. C. Chen, Y. S. Hsiao, F. C. Chien, P. Chen, C. H. Kuo, M. H. Huang and C. S. Hsu, *ACS Nano*, 2011, **5**, 959.
- 36 C. Pacholski, A. Kornowski and H. Weller, *Angew. Chem., Int. Ed.*, 2002, **41**, 1188.
- 37 W. J. E. Beek, M. M. Wienk, M. Kemerink, X. Yang and R. A. J. Janssen, *J. Phys. Chem. B*, 2005, **109**, 9505.
- 38 Y. Y. He, Z. Q. Li, J. F. Li, X. Y. Zhang, C. Y. Liu, H. Li, L. Shen, W. B. Guo and S. P. Ruan, *Appl. Phys. Lett.*, 2014, **105**, 223305.
- 39 X. H. Li, W. C. H. Choy, L. J. Huo, F. X. Xie, W. E. I. Sha, B. F. Ding, X. Guo, Y. F. Li, J. H. Hou, J. B. You and Y. Yang, *Adv. Mater.*, 2012, **24**, 3046.
- 40 Y. Y. He, C. Y. Liu, H. M. Jiang, W. B. Guo, L. Shen and W. Y. Chen, *Synth. Met.*, 2014, **195**, 117.
- 41 D. H. Wang, J. K. Kim, J. H. Seo, I. S. Park, B. H. Hong, J. H. Park and A. J. Heeger, *Angew. Chem., Int. Ed.*, 2013, **52**, 2874.
- 42 D. D. S. Fung, L. F. Qiao, W. C. H. Choy, C. D. Wang, W. E. I. Sha, F. X. Xie and S. L. He, *J. Mater. Chem.*, 2011, **21**, 16349.
- 43 E. D. Kosten, J. H. Atwater, J. Parsons, A. Polman and H. A. Atwater, *Light: Sci. Appl.*, 2013, **2**, e45.
- 44 C. C. D. Wang, W. C. H. Choy, C. Duan, D. D. S. Fung, W. E. I. Sha, F. X. Xie, F. Huang and Y. Cao, *J. Mater. Chem.*, 2012, **22**, 1206.
- 45 X. C. Li, F. X. Xie, S. Q. Zhang, J. H. Hou and W. C. Choy, *Light: Sci. Appl.*, 2015, **4**, e273.
- 46 G. Garcia-Belmonte, P. P. Boix, J. Bisquert, M. Sesolo and H. J. Bilink, *Sol. Energy Mater. Sol. Cells*, 2010, **94**, 366.
- 47 F. Fabregat-Santiago, G. Garcia-Belmonte, I. Mora-Seró and J. Bisquert, *Phys. Chem. Chem. Phys.*, 2011, **13**, 9083.